Chapter 2

Review of Terahertz Detectors

2.1 Introduction

The Terahertz detector is a type of transducer that converts the terahertz radiation into an electrical signal. Over the last seven decades, significant work has been carried out in the field of THz detectors and a variety of detection technologies for THz radiation have been developed. There has been significant progress made in the development of detectors that resulted in the opening up of the THz spectral region for a variety of applications. Some commonly used terahertz detectors are shown in Table 2.1.

Table 2.1 Typical Values of the THz detectors developed and used

Terahertz Detectors	**NEP (W/√Hz)**	**Voltage Responsivity (V/W)**	**Response Time (s)**	**Operating Temperature (K)**	**Bandwidth in THz band (THz)**
Bolometers [78]	10^{-16}-10^{-13}	10^{5}-10^{7}	10^{-2}-10^{-3}	≤ 4.2	0.1-30
HEB [79]-[80]	10^{-19}-10^{-17}	10^{9}	10^{-8}	≤ 0.3	0.1-30
Microbolometers [8], [55], [81]-[84]	10^{-11}-10^{-10}	10^{5}-10^{7}	10^{-7}-10^{-6}	≤ 300	0.1-30
Golay Cells [85]-[86]	10^{-10}-10^{-8}	10^{5}–10^{4}	10^{-2}	300	0.1-20
Pyroelectrics [87]	10^{-9}	10^{5}	10^{-2}	240-350	0.1-30
Schottky Diodes [88]	10^{-12}	10^{3}	10^{-11}	10-420	0.1-1.7

Silicon FETs [89]-[90]	10^{-11}	10^{2}	10^{-9}	10-420	0.1-4.3
HEMTs [91]	10^{-11}	10^{3}	10^{-11}	4.2-420	0.1-4

Commercially available detectors are cooled THz detectors (e.g., hot electron bolometers) and uncooled THz detectors (e.g., Golay cells and pyroelectric detectors). Some of the available detector technologies have been discussed in the next section.

2.2 A Few Current Detector Technologies

2.2.1 Bolometers

Bolometers are made of a resistive material that has high thermal conductivity and a small thermal capacity [83], [78], [92]. The typical structure of a bolometer is shown in Fig.2.1. The energy of the incident radiation on the detector is absorbed in the resistive material resulting in a change in the temperature and thereby causing a change in the resistance of the material [83]. This detection does not involve a photon interacting with an electron directly. Bolometer's response times can be slow because of the long response time, it gets an opportunity to cool down. However, this often limits bolometers to single-element detectors or small arrays requiring scanning techniques to produce an image and take data. As bolometers operate at cryogenic temperatures, they can achieve high sensitivities and detection of the entire THz frequency range (as shown in Table 2.1). The major disadvantage of a bolometer is that it is very slow to reset and hence not suitable for high-speed imaging and communication.

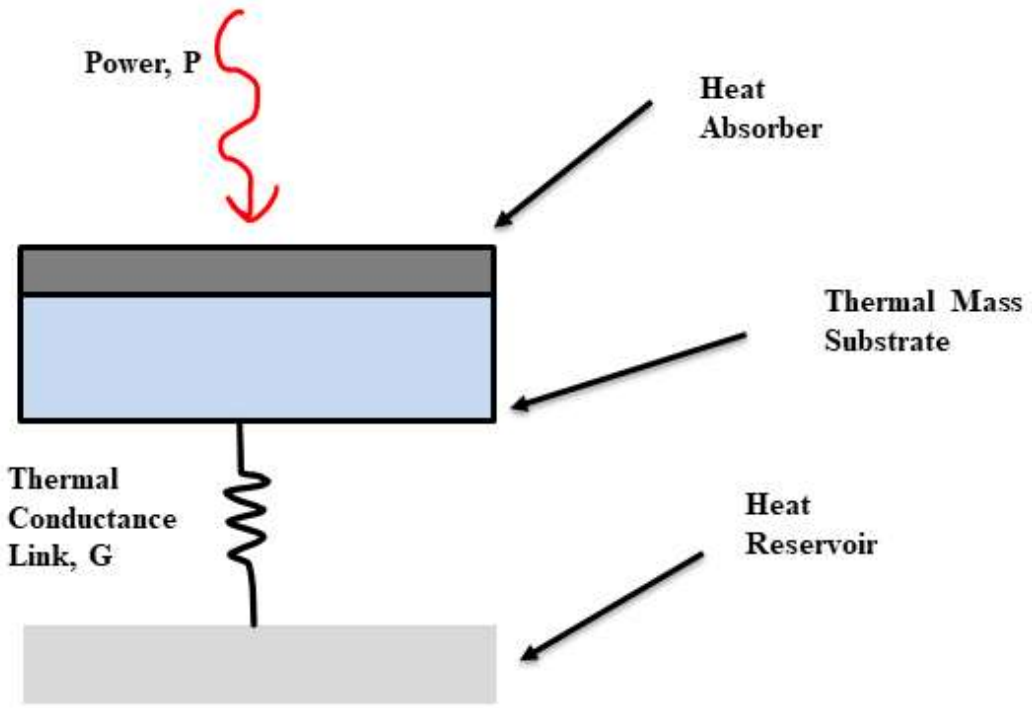

Fig.2.1 The schematic of a Bolometer

2.2.2 Microbolometers

Not all bolometers operate at cryogenic temperatures however, some can operate with high sensitivity even at room temperature. Microbolometer is one such type of room temperature bolometer. Microbolometers are the desired technology due to their ease of operation, reliability, sensitivity at room temperature, low cost, and ease of integration with silicon microcircuits. These are very useful for the creation of high-number focal plane arrays [87]. Recently, three companies namely NEC (Japan), INO (Canada), and CEA-LETI (France) have utilized the microbolometer properties for the design of commercialized high-density THz focal plane arrays. Microbolometers are typically built for operating at 8-14 microns. NEC, INO, and CEA-LETI have succeeded in detecting frequencies between 1 and 7 THz [84].

2.2.3 Pyroelectric Detector

A Pyroelectric detector is a type of room-temperature thermal detector. These detectors are available commercially for the entire range of IR as well as THz frequency regions. They are very cheap and rugged. Pyroelectric detectors are made of materials that change their dielectric constant as a function of the temperature, which increases with incident radiation. These detectors are exceedingly susceptible to heat and light interference [83]. The response of these detectors is also not well standardized and sensitivity can be limited. They can be made to respond quickly, but sensitivity will drop proportionately with faster response times in imaging, pollution detection, and gas analyzers [83].

2.2.4 Golay Cells

A Golay cell is also a room-temperature thermal detector. It consists of a gas cell, transparent window, lens system, flexible mirror, grid, and a detector as shown in Fig. 2.2. The gas cell is filled with a low thermal conductivity xenon gas. As seen in Fig.2.2, the gas cell is enclosed at one end by a transparent window and the other end by a very light flexible mirror. The gas cell contains a thin absorbing metallic film on the front end that transfers the energy from the radiation to the gas. When radiation of the desired frequency is incident on the transparent window, the radiation is absorbed by the metallic film. The gas inside the cell gets heated causing a change in the position of the flexible mirror. Light from the source is condensed by the lens system through a grid and is then reflected by the flexible mirror back through the grid onto the detector. Any movement of the mirror distorts the reflected image of the grid and changes the amount of light reaching the light detector. This is the basic working principle of a Golay cell. As it operates at room temperature, i.e., it does not require any cooling system,

its operational cost is low. It has a few disadvantages like it is fragile and extremely vulnerable to vibrational noise. It is also incredibly slow to respond, of the order of 15 milliseconds [83].

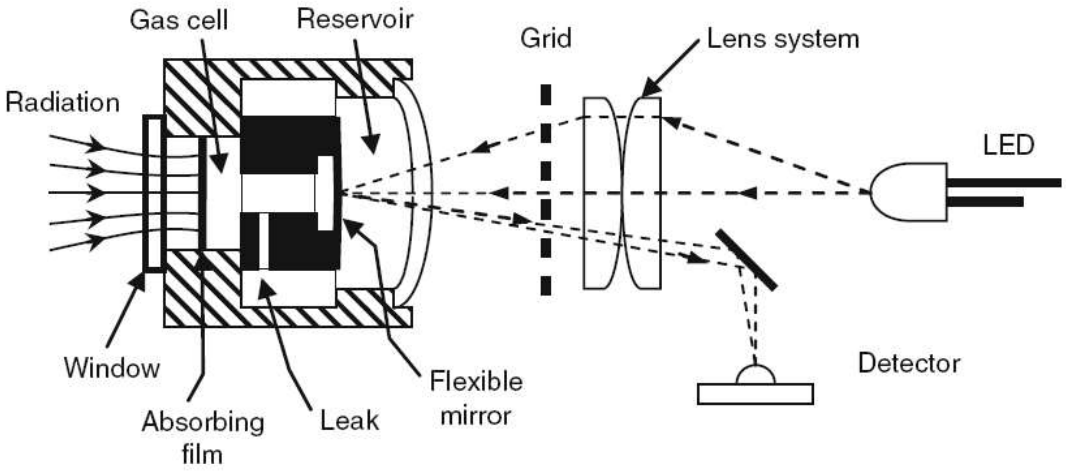

Fig.2.2 The schematic of a Golay Cell

2.2.5 Schottky Barrier Diodes

Schottky Barrier Diodes (SBDs) are the most used semiconductor devices in a coherent system. They can operate beyond 0.5 THz frequencies [83]. In SBDs, recombination rates become insignificant for determining the high-frequency cut-off. The reason for this is the dependence of nonlinear current-voltage characteristics on the transport of majority carriers. Therefore, the temperature has a negligible impact on the SBD characteristics, allowing it to work at room temperature, which is important for many applications [93]-[94]. The SBD detectors are primarily developed as single-pixel detectors since the fabrication process of arrays has significant performance fluctuations of devices [95]. The main problem with SBDs is that they are very fragile.

2.2.6 Graphene Detectors

Graphene is an allotrope of carbon. It is a fascinating material for terahertz applications with its strengths in atomic thickness, easy tunability, and high kinetic inductance [96]. Since the discovery of graphene, it has been extensively used in photodetection applications [97]. In pure form, it is having a zero bandgap. It is a semi-metal, unlike other metals due to the availability of free charge carriers that are induced by chemical doping due to its 2D nature. The opening of the bandgap of graphene through intentional substitutional doping, application of the electric field, and mechanical exfoliation has made it possible to use it in many semiconducting applications. Doping of the graphene results in a decrease in carrier mobility due to impurity scattering. Ryzhii *et al.* proposed a multi-layer graphene structure utilizing lateral p-i-n diodes (shown in Fig.2.3) for the detection in the THz region [98], [99]. They have used multi-layer graphene for the i-region. This structure exhibited substantially high responsivity and detectivity operating at room temperature. The photodetectors made with multi-layer graphene exhibited better efficiency than other detectors in the THz region. Of late, graphene is employed as a channel in the Field Effect Transistor (FET) structures for the detection of THz radiation. THz detectors that use the Photo-Thermoelectric Effect (PTE) [100] and antenna-coupled graphene FETs [101-103] at room temperatures were also reported. Yan *et al.* reported a hot electron bolometer (shown in Fig.2.4) using bilayer graphene [104]. A perpendicular electric field applied resulted in the development of electron-temperature-dependent resistance at low temperatures thus making it useful in thermometry. The key problems with graphene are that it has a very low optical absorption and has low carrier lifetime. In the literature, mainly graphene detectors experimentally reported were operated above 100 μm wavelength i.e., below 3 THz frequency.

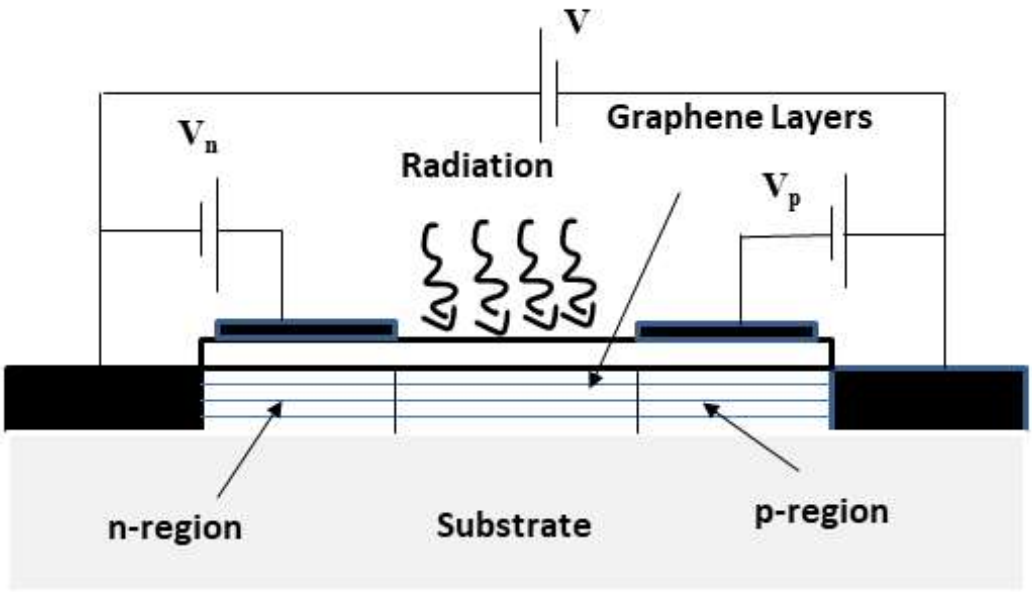

Fig.2.3 The schematic of a Graphene-based p-i-n Photodetector

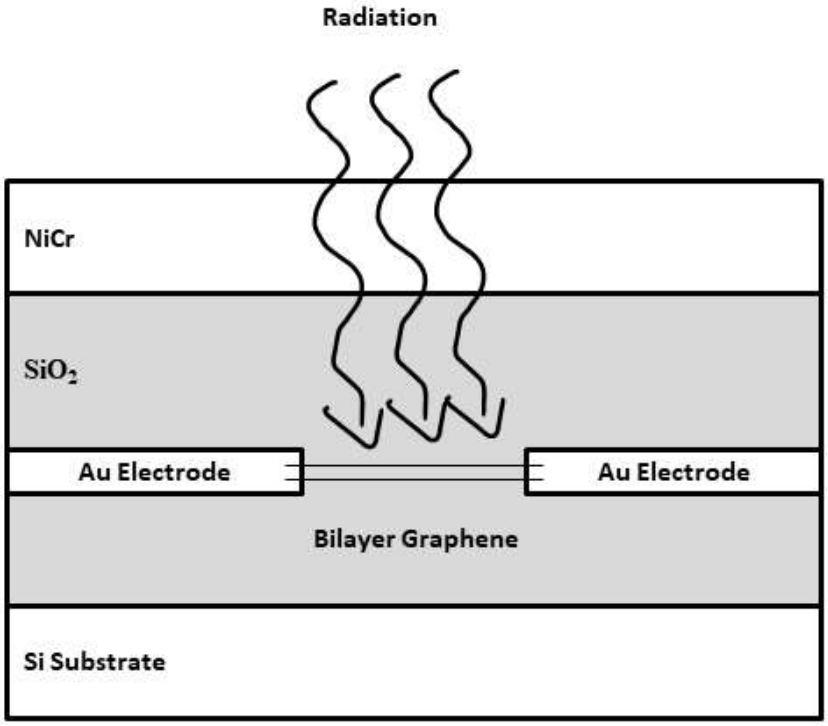

Fig.2.4 The schematic of a Bilayer Graphene Hot-Electron Bolometer

2.3 State-of-the-art THz Detectors

The major requirement of any communication system is speed. The thermal detectors discussed in the above section suffer from the low speed of operation in the THz region. This problem can be avoided by employing junction devices like p-n diodes, p-i-n diodes, and other junction transistors like MESFET. One of the popular materials used for the development of detectors in the infrared region and some parts of the THz region is the mercury cadmium telluride (MCT) which offers high speed for a communication system. MCT possesses unique properties that are advantageous in the development of detectors in the THz region. The importance of MCT material and its properties have been discussed in the next section.

2.3.1 Mercury Cadmium Telluride

The publication by Lawson and his colleagues in 1959 sparked the creation of variable-bandgap HgCdTe alloys, enabling a supreme level of design freedom for IR detectors [105]. The focus of HgCdTe technology development is primarily on military applications. The accompanying restrictions for secrecy that prevent fruitful interactions among research teams on a national and especially worldwide level have been a drawback of supporting defence agencies. Nevertheless, over the past 40 years, a lot of development has been accomplished. The most popular variable-gap semiconductor for IR photodetectors right now is HgCdTe. Despite having successfully repelled significant threats from extrinsic silicon and lead-tin telluride devices throughout the years, it now faces more rivals than ever. These include Schottky barriers on silicon, SiGe heterojunctions, AlGaAs multiple quantum wells, GaInSb strain layer superlattices, high-temperature superconductors, and especially two types of thermal detectors pyroelectric detectors and silicon bolometers. However, it is intriguing that none of these rivals can compete in terms of fundamental characteristics. Except for thermal

detectors, they might promise to be more easily manufactured while also delivering better performance or operating at higher or even equivalent temperatures. Making a high-performance HgCdTe photodetector, however, faces several challenges. The fabrication of the material with the necessary purity is a major challenge. High-purity HgCdTe has been produced using growth processes such as molecular beam epitaxy (MBE) and liquid phase epitaxy (LPE). HgCdTe can be used for detectors that are controlled in a variety of ways, and it can be tailored for operation at temperatures ranging from liquid helium to room temperature as well as an incredibly large range of wavelengths (1-30 μm).

The material quality has reached the level of maturity required to produce electronically scanned large-area focal planes for high-quality thermal imagers. The elements of the present liquid nitrogen-cooled arrays achieve the theoretical performance level. Technological issues, not fundamental limits, are all that keep HgCdTe from completely dominating almost all IR applications. The key issues are uniformity, producibility, and cost.

2.3.2 Material Properties of MCT

$Hg_{1-x}Cd_xTe$ is a ternary compound narrow bandgap semiconductor. It is the third most studied semiconductor after Silicon and Gallium Arsenide. It is a very attractive material for its unique properties and has been receiving a lot of interest in the scientific community over the past few decades. The ternary compound $Hg_{1-x}Cd_xTe$ is formed from the combination of binary compounds CdTe and HgTe by Vegard's law. CdTe and HgTe have zinc-blende structures. For all values of x, $Hg_{1-x}Cd_xTe$ also has a zinc-blende structure.

2.3.2.1 Crystal structure

HgTe and CdTe crystallize in a zinc blende structure which is composed of two interpenetrating fcc sub lattices displaced by (1/4a, 1/4a, 1/4a) along the cubic body diagonal, a is the lattice constant. Let the compound be AB, A is the cation and B is the anion. The A atoms occupy sites of one of these fcc sub lattices and the B atoms occupy the sites on the other. The crystal bonding is mainly covalent (tetrahedrally directed bonds) and partially ionic also. In $Hg_{1-x}Cd_xTe$, cations are of two different species e.g., A', A'' species, representing the material generically as $A'_{1-x}A''_xB$. The A' and A'' species are distributed randomly over the lattice sites in the crystal.

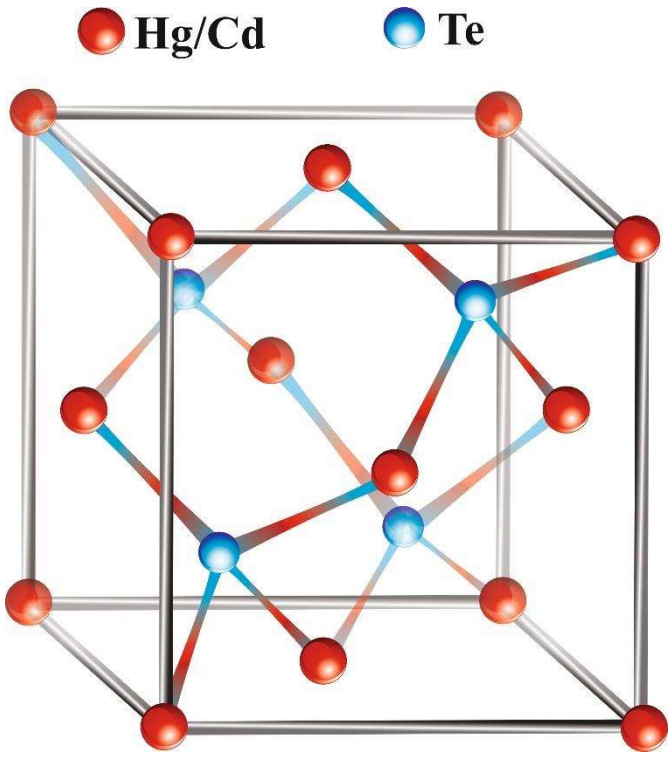

Fig.2.5 Lattice structure of mercury cadmium telluride

2.3.2.2 Band Structure

The II-VI ternary alloys crystallize in a zinc blend structure. The valence electrons in these semiconductors form a covalent bond and the quasi-continuum of levels that they occupy is the valence band (contains 8 electrons per unit cell). The typical band structure of a zinc blend MCT structure is shown in Fig.2.6.

The fundamental absorption edge corresponds to direct transitions from the highest valence band at Γ point ($k_p = 0$) to the lowest conduction band at X point. The lowest bandgap transitions occur at the center of the Brillouin zone. Away from $k_p = 0$, the valence band is split into the heavy hole, light hole, and split-off branches labeled as hhv, lhv, and sov respectively. The energy gap can be considered direct, with both band extrema being at the same point in k_p-space.

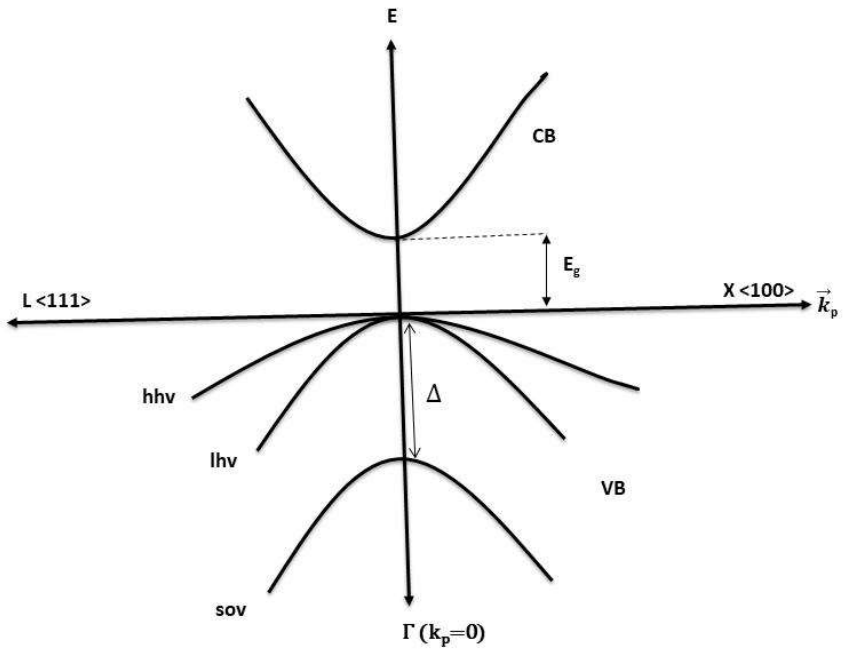

Fig.2.6 E-k_p diagram of mercury cadmium telluride

The electrical and optical properties of the MCT can be explained in the same way as InSb by the energy gap structure in the vicinity of the Γ-point of the Brillouin zone. The shape of the electron band and the light-mass hole band are determined by the $\boldsymbol{k \cdot p}$ interaction, and hence, by the energy gap and the momentum matrix element. There are several expressions available to represent the variation of energy bandgap with the alloy composition and temperature. The most widely used empirical formula for determining the energy bandgap value of $Hg_{1-x}Cd_xTe$ in terms of composition (x) and temperature is given by [106]

$$E_g(eV) = -0.302 + 1.93x - 0.810x^2 + 0.832x^3 + 5.35 \times 10^{-4}(1-2x)\left\{\frac{-1822 + T^3}{255.2 + T^2}\right\} \quad (2.1)$$

Fig.2.7 shows the variation of energy bandgap with the mole fraction. It can be seen from the figure that for low mole fractions, the behaviour of the material changes from semiconductor to metal. In general, at a temperature of 77 K, CdTe has an energy bandgap value of 1.6088 eV and HgTe has an energy band gap value of –0.2608 eV. As the value of x changes from 1 to 0, the bandgap shifts from the CdTe energy bandgap to the HgTe energy band gap.

Fig.2.7 shows the variation of energy bandgap with the mole fraction. It can be seen from the figure that for low mole fractions, the behaviour of the material changes from semiconductor to metal. In general, at a temperature of 77 K, CdTe has an energy bandgap value of 1.6088 eV and HgTe has an energy band gap value of –0.2608 eV. As the value of x changes from 1 to 0, the bandgap shifts from the CdTe energy bandgap to the HgTe energy band gap.

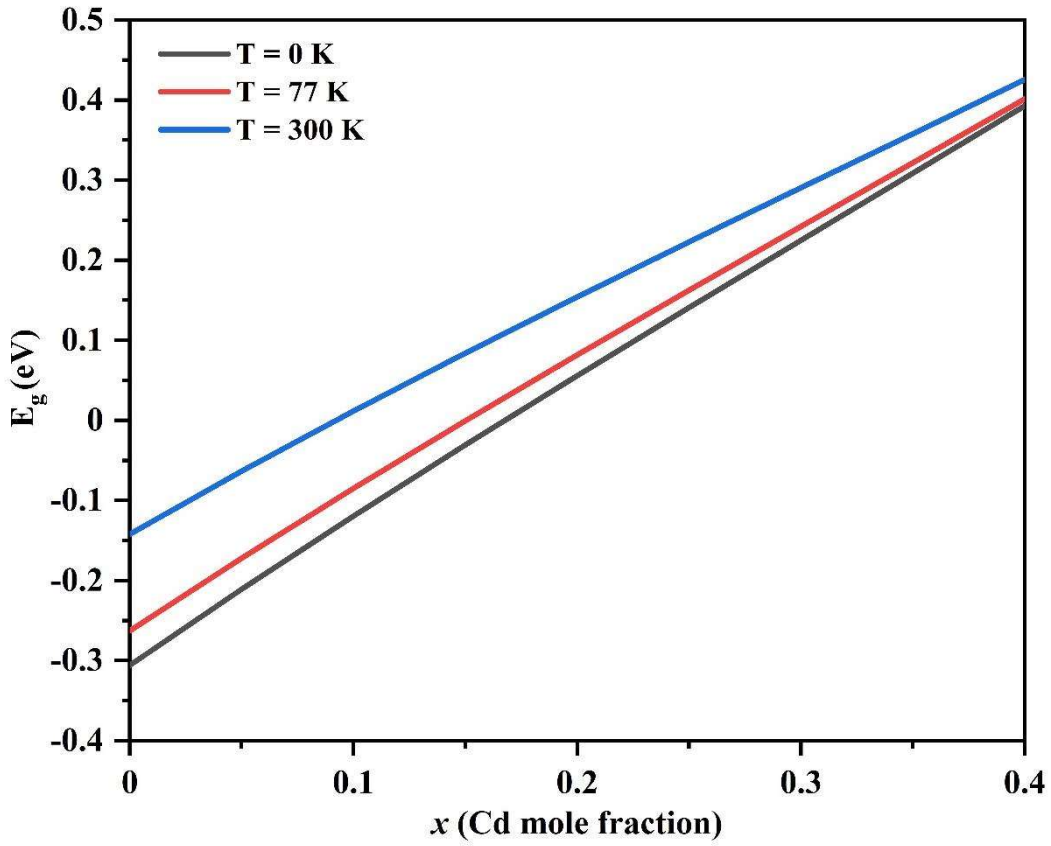

Fig.2.7 Energy bandgap of HgCdTe versus Cd mole fraction under different temperatures

HgCdTe is a semiconductor that covers the entire IR region of the electromagnetic spectrum for a small change in the lattice constant [107]. A desirable property of MCT is almost negligible change in the lattice constant as a function of *x*.

The variation of the lattice constant (a) of MCT with the change in the mole fraction (x) is given by [108]

$$a = 6.4614 + 0.0084x + 0.01168x^2 - 0.0057x^3 \quad (2.2)$$

The lattice constant is expressed in Angstroms (Å)

It can be seen in Fig.2.8, that the lattice constant of CdTe (x=1) is only 0.3 % larger than that of HgTe (x=0). This is very critical because slight variations in the lattice constant allow for

the creation of novel devices based on lattice-matched high-quality complicated epitaxial layers.

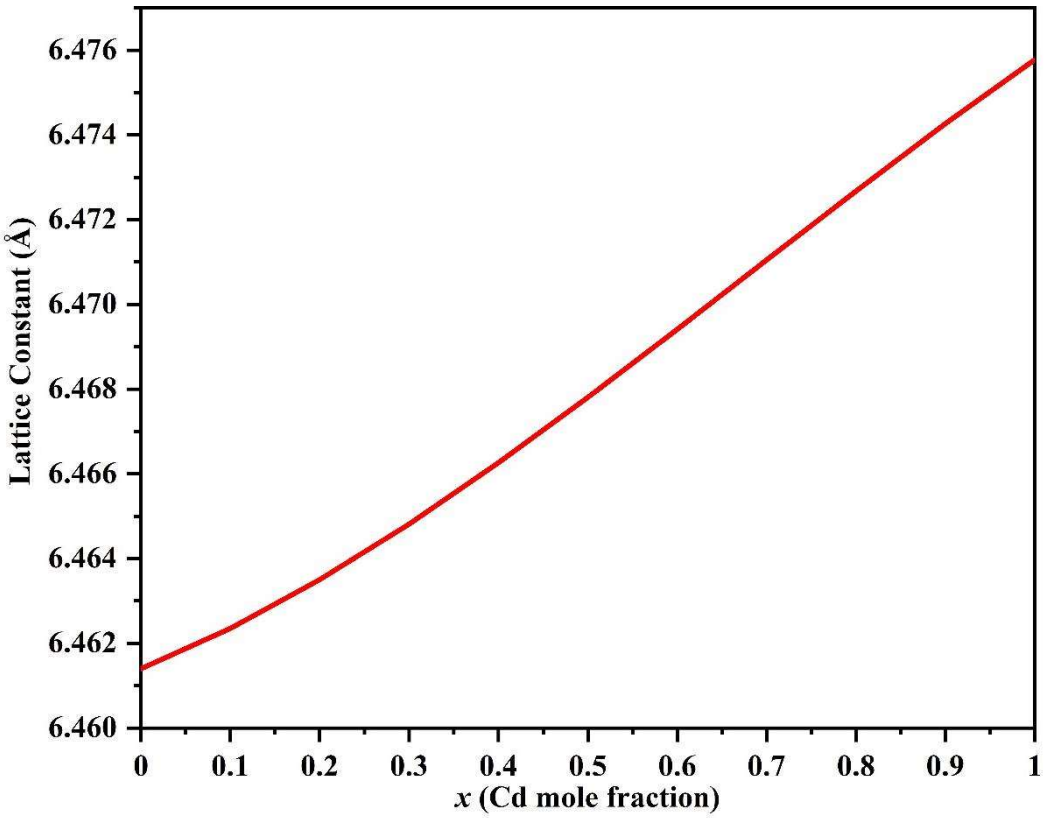

Fig.2.8 Variation of lattice constant with *x* (Cd mole fraction)

The expression for the intrinsic carrier concentration of HgCdTe is given by [109]

$$n_i(/m^3) = (5.24256 - 3.57290x - 4.74019 \times 10^{-4}T + 1.25942 \times 10^{-2}xT - 5.77046x^2 - 4.24123 \times 10^{-6}T^2) \times 10^{20} E_g^{\frac{3}{4}} T^{\frac{3}{2}} exp\left(-\frac{E_g}{2kT}\right) \quad (2.3)$$

The intrinsic carrier concentration becomes quite large with the increase in temperature. Therefore, the doping concentration of the absorber material should be as low as possible to minimize the effect of recombination and maximize the minority carrier diffusion length. If the doping concentration is large in the absorbing layer of any photodetector, it can cause significant Auger processes and reduced minority carrier diffusion length. Considering the

above factors, the detector should be designed in such a way that it does not become intrinsic at the operating temperature.

The electron affinity (χ) of HgCdTe is computed from the following empirical expression [110]

$$\chi(eV) = 4.23 - 0.813 \times (E_g - 0.083) \tag{2.4}$$

The electron effective mass (m_n^*) of HgCdTe material is calculated by Weiler's expression [111]

$$m_n^* = m_0 \left(1 + 2F + \frac{E_p}{3}\left(\frac{2}{E_g} + \frac{1}{E_g + \Delta}\right)\right)^{-1} \tag{2.5}$$

where $E_p = 19\ eV$, $\Delta = 1\ eV$ and $F = -0.8$. and the hole effective mass is high usually measured in the range between 0.3-0.7m_0. Usually in the modeling of the photodetectors, $m_p^* = 0.55m_0$ is used.

Since the effective electron mass is low, the electron mobility of HgCdTe is significantly high.

The electron mobilities of MCT are relatively very high due to the low effective masses. Electron mobility of MCT depends on the temperature and the bandgap. The empirical expression for electron mobility (μ_n) is given by [112]

$$\mu_n(m^2/Vs) = \frac{9 \times 10^4 s}{T^{2r}} \tag{2.6}$$

where $r = \left(\frac{0.2}{x}\right)^{0.6}$ and $s = \left(\frac{0.2}{x}\right)^{7.5}$

The hole mobility (μ_p) is expressed empirically as follows [112]

$$\mu_p(m^2/Vs) = \mu_o \left[1 + \left(\frac{p}{1.8 \times 10^{23}}\right)^2\right]^{-\frac{1}{4}} \tag{2.7}$$

where $\mu_0 = 0.044\ m^2/Vs$ and p is the acceptor impurity concentration in m^{-3}.

The hole mobility of HgCdTe is computed by presuming the electron-to-mobility ratio equal to 100.

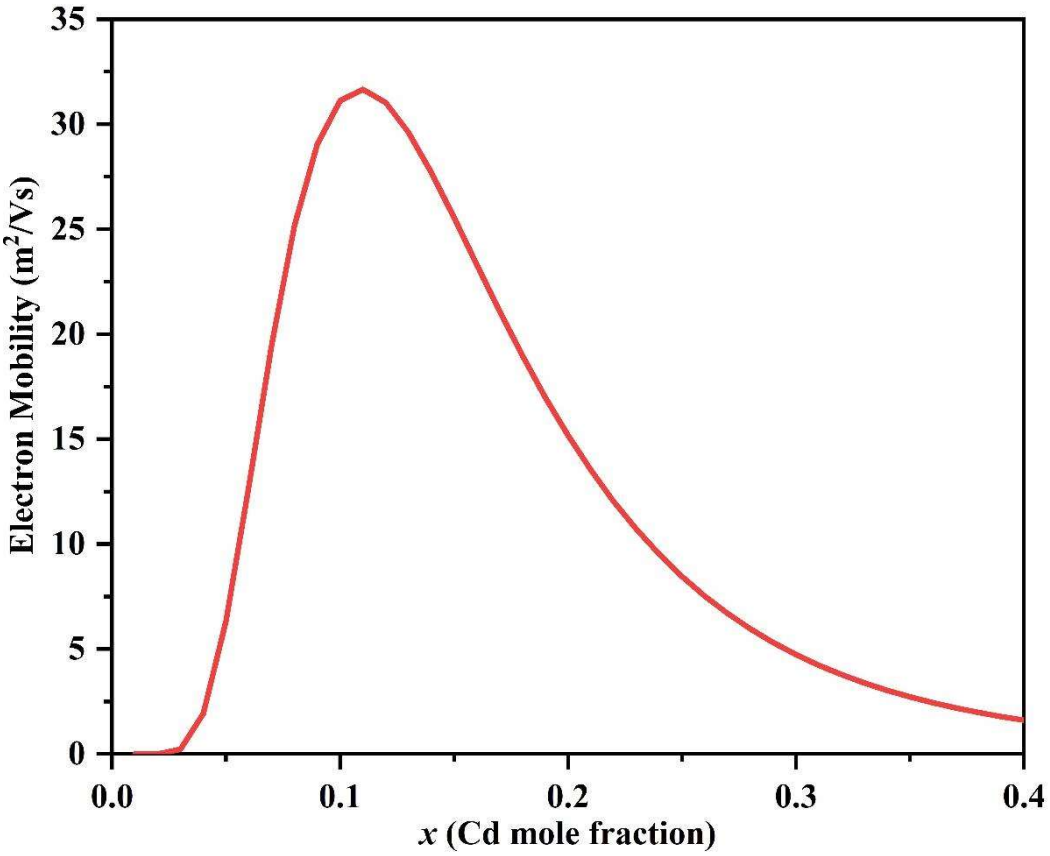

Fig.2.9 Electron Mobility of HgCdTe versus *x* (Cd mole fraction) at a temperature of 77 K

As can be seen from Fig.2.9, the electron mobility decreases with the increase in the *x* composition. On the other hand, for lower values of *x* composition, the mobility increases with the increase in the *x* composition.

2.3.2.3 Optical Properties

HgCdTe has a very high absorption coefficient (α) for a wide range of compositions. Moreover, it has a high ratio of optical generation to thermal generation rate which makes it a suitable material for IR and terahertz detectors. For narrow bandgap semiconductors, the absorption coefficient depends on the doping and the temperature. Because of the Moss Burstein shift of the Fermi level, the absorption edge is pushed to higher energies and the apparent bandgap is increased. However, long wavelength photon absorption is significant in HgCdTe resulting in exponential band tailing at energies lower than bandgap. Close to the band edges, there are many defect states in the gap, which give rise to appreciable absorption with photon energies lower than E_g. For large *x*, excitons give rise to discrete energy levels within the band.

The exponential band tail absorption below E_g is referred to as Urbach's tail and is expressed as [113]

$$\alpha\ (m^{-1}) = 100 * \alpha_0 exp\left(\frac{\delta(E - E_0)}{kT}\right) \tag{2.8}$$

where $\alpha_0 = -18.5 + 45.68x$

$$E_0(eV) = -0.355 - 1.77x$$

$$\frac{\delta}{kT} = \frac{\ln \alpha_g - \ln \alpha_0}{E_g - E_0}$$

$$\alpha_g = -65 + 1.88T + (8694 - 10.315T)x$$

It can be seen from Fig.2.10 that the material MCT has high values of the absorption coefficient for various wavelengths.

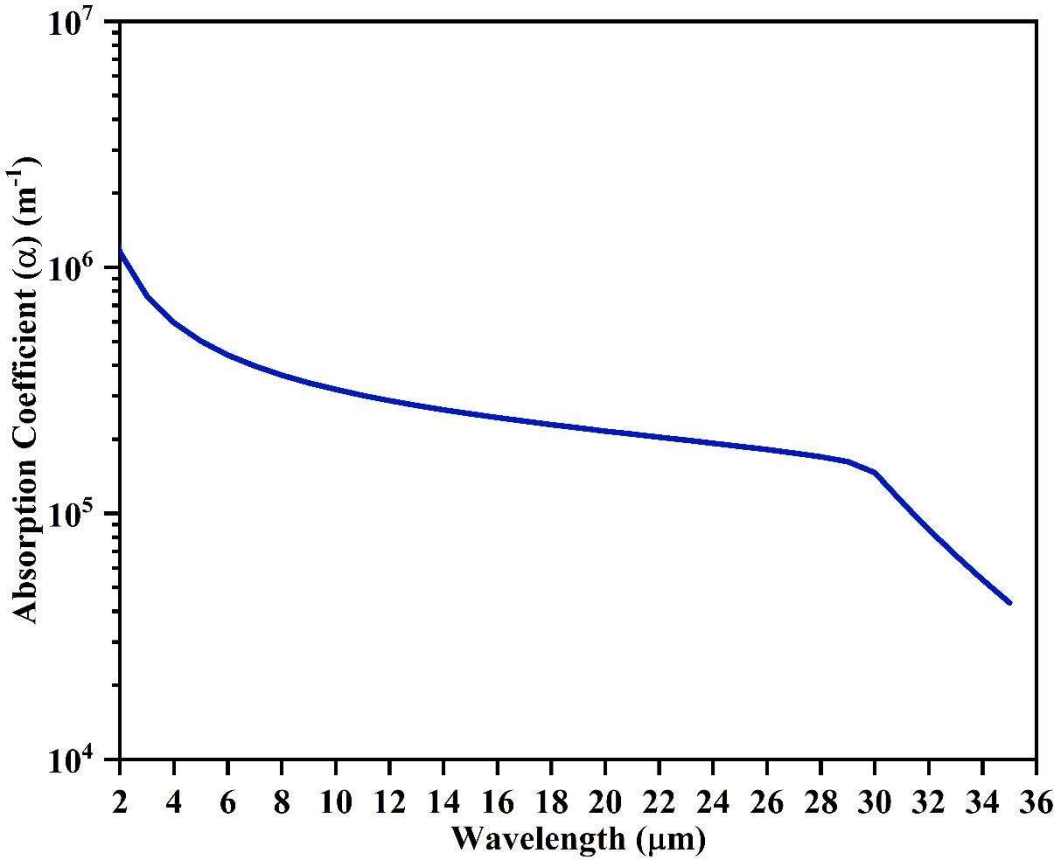

Fig.2.10 Absorption coefficient of HgCdTe for $x = 0.175325$ versus wavelength at 77 K

The refractive index (n) of the HgCdTe is estimated based on the following empirical formula [107]

$$n^2(\lambda, T) = A + \frac{B}{1 - \left(\frac{C}{\lambda}\right)^2} + D\lambda^2 \tag{2.9}$$

where A, B, C, and D are the fitting parameters that vary with the composition x and temperature T

$$A = 13.173 - 9.582x + 2.909x^2 + 10^{-3}(300 - T)$$
$$B = 0.83 - 0.246x - 0.0961x^2 + 8 * 10^{-4}(300 - T)$$
$$C = 6.706 - 14.437x + 8.531x^2 + 7 * 10^{-4}(300 - T)$$
$$D = 1.953 * 10^{-4} - 0.00128x + 1.853 * 10^{-4}x^2$$

The two dielectric constants e.g., the high-frequency dielectric constant (ϵ_∞) and the static dielectric constant (ϵ_s) have been derived from the reflectivity data in evaluating the real and the imaginary parts of ε [114].

$$\epsilon_\infty = 15.2 - 15.6x + 8.2x^2 \tag{2.10}$$

$$\epsilon_s = 20.5 - 15.6x + 5.7x^2 \tag{2.11}$$

The cut-off wavelength is obtained based on the following expression

$$\lambda_c(\mu m) = \frac{1.24}{E_g(eV)} \tag{2.12}$$

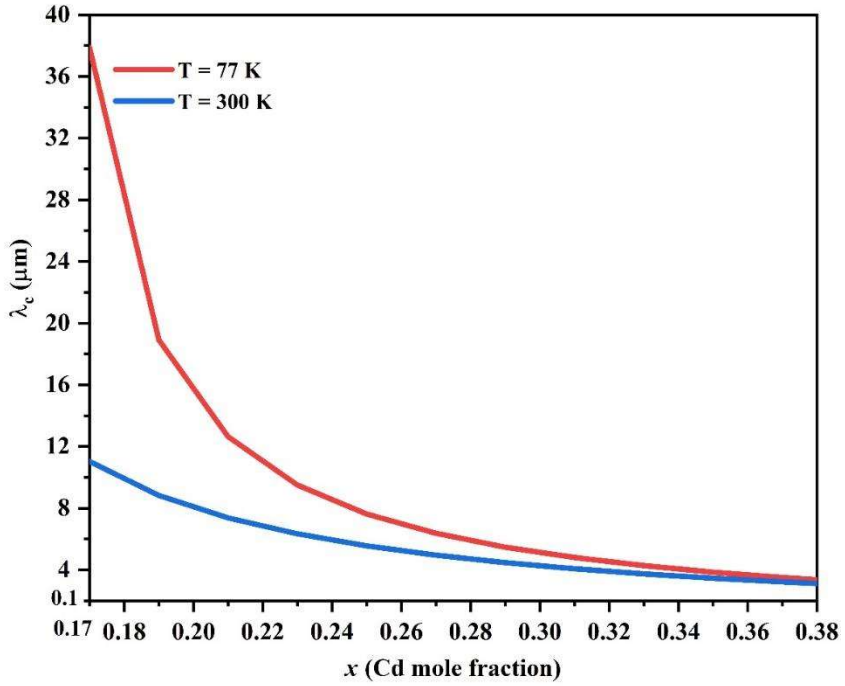

Fig.2.11 Cut-off wavelength of HgCdTe as a function of *x* (Cd mole fraction)

In Fig.2.11, the x-composition is varied from x =0.17 to $x = 0.38$. By using equation 2.1, we can able to compute the energy bandgap. From equation 2.12, the cut-off wavelength is found to be $\lambda_c = 38\ \mu m$ at $x = 0.17$ at a temperature of 77 K and $\lambda_c = 11\ \mu m$ for the same composition but at a temperature of 300 K. As the x-composition decreases further, the behaviour of HgCdTe changes from semiconductor to metal.

As seen in Fig.2.11, for low temperatures i.e. at 77 K, it is possible to detect longer wavelengths. At higher temperatures, it is difficult to control the thermally generated carriers. Hence to control these carriers, a cryogenic cooling technique is employed for better performance of the devices. So, for wavelengths (10 μm) and beyond, it is not possible to fabricate devices at 300 K.

2.4 Need for cooling

Usually at room temperatures, the thermal energy of the charge carriers becomes comparable to the narrow bandgap of MCT. The thermally generated carriers start competing with the optically generated carriers in the MCT. Therefore, the thermal generation process dominates the optical generation. Inherent thermal generation-recombination processes such as Auger, Shockley Read Hall recombination, band-to-band, and trap-assisted tunneling mechanisms contribute to the dark current and hence to the noise of the detector, especially for higher-order wavelengths i.e., LWIR and beyond. To reduce the noise, it is necessary to use liquid nitrogen cooling or liquid hydrogen cooling based on the requirement.

From the literature survey, it was found that very few detectors are available based on MCT operating in the THz region. They have been listed in Table 2.2.

Table 2.2 Detectors based on MCT in the THz region

Device	η (%)	ℜ (A/W)	D* ($mHz^{1/2}$ W^{-1})	NEP ($W/Hz^{1/2}$)	Temperature (K)	Frequency (THz)
MCT-based photodetector [115]	80	--	8×10^{9}	--	77	30
MCT-based heterojunction photodetector [116]	80	6.75	2.25×10^{11}	1×10^{-7}	77	30
MCT-based Bolometer [117]	--	--	--	2.5×10^{-10}	300	0.14
MCT-based THz and IR detector [118]	--	--	--	4.5×10^{-10} 5×10^{-9}	300 77	0.14

* η – Quantum Efficiency, ℜ - Responsivity, D* - Specific Detectivity and NEP – Noise Equivalent Power

The major challenges associated with the MCT-based devices in THz region are as follows:

- Growth of the material free of defects.
- Finding compatible materials for formation of contacts.
- Operation of the devices at room temperature.
- Reduction of cost of fabrication.

2.5 Motivation

Since the discovery of MCT, it has been used for short, mid, and long-wavelength infrared detection purposes. Although MCT can be used beyond 10 μm wavelengths, it has not been

explored yet. There is a research gap for the exploration in the development of the devices based on MCT in the THz region as most of the bolometric devices having a wideband operation over the entire THz region face slow response. So far, from the discussion, we observed that the MCT properties can be varied based on the material composition and temperature. A slight variation in the *x*-composition results in a complete change of behaviour of the material from semiconductor to semi-metal especially for low compositions. Therefore, based on the unique material properties of MCT, availability, improved technology for its growth, its compatibility with materials, and despite its limitation for cryogenic cooling, a study on the devices based on MCT in the THz region have been taken up. The detailed analysis of different THz structures based on MCT has been carried out in the next chapters. This thesis is limited to the design and study of the THz detectors based on MCT for the operating wavelength of 30 μm.